



# Multifractal modelling of electrochemical noise in corrosion of carbon steel

S.V. Muniandy<sup>a,\*</sup>, W.X. Chew<sup>a</sup>, C.S. Kan<sup>b</sup>

<sup>a</sup> Plasma Research Laboratory, Department of Physics, University of Malaya, 50603 Kuala Lumpur, Malaysia

<sup>b</sup> ASEPTec SDN BHD, Taman Equine, Bandar Putra Permai, 43300 Seri Kembangan, Selangor, Malaysia

## ARTICLE INFO

### Article history:

Received 25 May 2010

Accepted 4 September 2010

Available online 16 September 2010

### Keywords:

A. Steel

B. Potentiostatic

B. Modelling studies

## ABSTRACT

Electrochemical noise analysis of corroding surfaces provides useful information regarding the temporal changes in material degradation, corrosion mechanisms and condition monitoring. In this study, we analyzed the electrochemical potential and current noise originating from the corrosion of carbon steel (ASTM A106) in distilled water using multifractal analysis. The empirical Legendre spectrum and large deviation singularity spectrum are determined for the electrochemical noise at different stages of corrosion. A wavelet-based multifractal model is introduced to describe the multiscaling behaviour.

© 2010 Elsevier Ltd. All rights reserved.

## 1. Introduction

Corrosion is deterioration of essential properties in a material due to reactions with its surrounding [1,2]. It is an electrochemical process whereby metal reacts with its environment to form an oxide or other compound. When metal is exposed to an electrolyte, the metal atoms at the anode site lose electrons and these electrons are then absorbed by other metal atoms at the cathode site. There are many techniques to monitor corrosion processes, which can be classified in two ways – intrusive/non-intrusive and direct/indirect methods [3,4]. An intrusive and direct technique requires entry into the process stream and measures the direct result of corrosion. Examples of such methods include the corrosion coupons, electrical resistance, linear polarization resistance, electrochemical noise analysis, etc. Techniques such as ultrasonic testing and radiography are considered as indirect corrosion monitoring techniques as they could only measure the outcome of the corrosion process. One of the versatile direct techniques mentioned above is the electrochemical noise (EN) analysis which has been proved useful for studying corrosion processes. EN is generally defined as random fluctuations of the potential or current observed in corrosion processes [5–7]. The fluctuation can be regarded as a result of the random nature of the corrosion reactions. This method is attractive in corrosion monitoring applications because of the non-intrusive measurement technique.

However, the interpretation of data from electrochemical noise measurement requires detailed analysis as it often contains complex superposition of different signatures and irregular fluctuations. In terms of signal's characteristic harmonics, these may

refer to low-frequency (large time scale) and high-frequency (small time scale) information contents. The presence of various mechanisms with broad range of time scales is likely to complicate the analysis of EN signals. The main objective of this study is to analyze the electrochemical potential and current noise originating from the corrosion of carbon steel (ASTM A106) in distilled water using multiscaling analysis, namely  $q$ th order wavelet scalogram [8] and multifractal analysis [9,10]. One of the main results of the study is the introduction of multifractal wavelet model for simulating small time scale fluctuation using beta-distributed random multiplicative cascade process [11]. The paper is organized as follows. In Section 2, we briefly introduce the corrosion monitoring techniques with emphasize on EN. Characterization of EN signals using Fourier power spectral density and wavelet scalogram based on spectral amplitudes, spectral exponents, Hurst or Holder exponents and fractal dimensions are described in Section 3. The experimental setup for measuring the EN potential and current noise is given in Section 4. Scaling behaviour of EN signals from the perspective of fractal and multifractal theories are described in Section 5. The results of the parameters estimation and simulation are discussed in Section 6 before the conclusion.

## 2. Corrosion monitoring using EN

Various studies have indicated that the EN is able to provide valuable information about corrosion types and mechanisms [12–21]. Basically, there exist two general classes of corrosion, namely the uniform and the localized corrosion. Uniform corrosion takes place evenly across the entire exposed surface of the metal. Localized corrosion in contrast, is concentrated to small areas of exposed surface and often results in deep penetration of the material. Since the net corrosion rate is lower than that of uniform

\* Corresponding author. Tel.: +60 3 79674292; fax: +60 3 79674146.

E-mail address: [msithi@um.edu.my](mailto:msithi@um.edu.my) (S.V. Muniandy).

corrosion, detailed analysis techniques are needed for monitoring localized corrosion. In order to understand the mechanism of corrosion, the source of EN can be traced to three main components, namely the charge carrier effects, surface processes and environmental changes. Carrier induced noise originates mainly from the discrete nature of charge and its thermal agitation. Noise due to surface processes occurs on the electrodes and specifically to their heterogeneity. Variations in the physical and chemical parameters of the observed system contribute to the very slow fluctuations of the electrode potential.

Uniform corrosion of iron and iron alloy in various saline solutions have been extensively studied based on EN characteristics by Legat and Zevnik [22] and many others [23,24]. Corrosion process tends to be localized when the solution is still, while in system with strong movement of electrolyte, the tendency is towards uniform corrosion [25]. Corrosion of metals and alloys by pitting constitutes one of the serious material damages. Pitting is an electrochemical process in which small holes grow rapidly in a metal surface under the influence of a electrolytic anion and an electric field. The origin of the nucleation site depends on a number of factors regarding the system. EN based techniques are proven to be sensitive for detecting spontaneous changes in the corrosion processes namely the initiation of pitting and cavitations attack [26,27]. Some metallurgical microstructural or microcompositional features may induce pitting preferentially, for example in stainless steel in chloride solution, where as in the case of aluminium ion migration under the electric field is required [28,29]. Other forms of corrosion include crevice corrosion, intercrystalline corrosion, stress corrosion cracking, etc. [30].

As this study is focusing on corrosion in carbon steel, some recent findings related to EN are briefly described. Carbon steel accounts for approximately 85% of the annual steel production worldwide and becomes the most widely used engineering material, despite its relatively limited corrosion resistance [31]. Mild steel and high carbon steels are classified as ferrous metals (with large percentage of iron) which can be further subdivided as (a) mild or low carbon steel (0.08–0.30% carbon), (b) medium carbon steel (0.3–0.5% carbon) and high carbon steel (0.55–1.40% carbon). While they may occur small changes in the general corrosion behaviour among the different types of carbon steel, small additions of copper, chromium, nickel and phosphorous are known to produce significant reduction in corrosion rate in certain environments. Aqueous corrosion of carbon steel under different experimental conditions can be found in [22,32–34]. Corrosion of pipes carrying tap water has been found to be accelerated by increase in both the temperature and the oxygen content of the water and sometimes by changes in its chemical composition. The corrosion rate of carbon steel is also observed to be strongly dependent on the pH and fluid velocity [35]. Characteristic of EN in carbon steel corrosions in the presence of different corrosion inhibitors have been considered in [36–39]. The atmospheric corrosion of carbon steel depends on relative humidity and time of exposure in the environment containing corrosive gases such as  $\text{SO}_2$ ,  $\text{NO}_x$ ,  $\text{CO}_2$ ,  $\text{O}_3$ ,  $\text{NH}_3$ , etc. [40]. Reduction in the atmospheric corrosion rate of carbon steel has been observed by alloying the steel with copper, nickel, silicon, chromium and phosphorous. We end this section with a remark that very little is known about corrosion in carbon steel in distilled water. Therefore, this study is hoped to highlight some non-trivial aspects of EN signals in such a system, in particular the scaling behaviour.

### 3. Scaling approaches in EN analysis

There are various types of time series analysis techniques developed to extract useful information such as corrosion types and corrosion rate from the electrochemical signals. Among the commonly

used EN analysis approaches are time-domain statistics [5,7] such as mean, variance, skewness, kurtosis, root-mean-square and the frequency domain power spectrum density [41]. Pujar et al. [42] used standard deviation of current noise versus time to assess intergranular corrosion in 316(N) stainless steel. Hladky and Dawson [41] showed that the amplitude of EN power spectrum at low-frequency is correlated to the rate and mode of corrosion attack. Moreover, a characteristic roll-off slope of the power spectral density was shown to be related to the type of corrosion [41,43,44]. For example, in [41], a roll-off of  $-20$  dB/decade was associated to with pitting attack while a much steep roll-off  $-40$  dB/decade was observed in cases where general corrosion processes are predominant. From the perspective of fractal geometry, the roll-off slope refers to power-law type scaling phenomenon [9,45]. Hence, the spectral exponent  $\beta$  of the power spectral density can be related to the fractal dimension  $D$  through a relation  $D = (5 - \beta)/2$ . A concrete fractal stochastic process that exhibits such a ubiquitous characteristic is fractional Brownian motion parameterized by self-similar exponent  $H$  (also known as Hurst exponent), where  $0 < H < 1$  [46]. The Hurst exponent is related to fractal dimension by relation  $D = 2 - H$  or with spectral exponent  $\beta$  by  $\beta = 2H + 1$ . Estimation of Hurst exponent can be done based on linear regression of log-log plot of power spectral density or using the rescaled-range (R/S) analysis. R/S analysis has been used to study spontaneous voltage fluctuation in 7039-T64 and 2519 aluminium alloy specimens in aerated NaCl solution [47]. The fractal dimension and the Hurst exponent were then compared with the results of electrochemical impedance spectroscopy and surface microscopy to determine the severity of localized attack of aluminium. Following the interpretation of a fractal stochastic process with long-range dependence, the noise is said to be anti-persistent when  $H < 1/2$  and persistent when  $H > 1/2$ . The crossover from persistent to anti-persistent is observed at large time scales in the corrosion of aluminium in electrolyte containing NaCl [48]. The anti-persistent nature of pitting above the crossover time indicates that each pit influences the potential such a way that it impedes the formation of a new pit. Despite the success of power spectral density analysis for EN characterization, the method has a serious limitation, namely it is valid only when the signal is stationary. Most often, the EN signals are highly non-stationary with complex scaling behaviour, especially when the localized corrosion starts to occur with pitting initiation and pitting propagation. To overcome the limitations of fast Fourier transform-based approaches, one can resort to the more powerful wavelet-based analysis which enables the characterization of non-stationary properties of the EN signal such as local point-wise regularity [8], and also capable of providing time-varying spectral analysis.

The multiresolution property of wavelet analysis is a powerful tool to detect local regularity and self-similar scaling features. There are a number of studies that have already highlighted the fractal characteristic of EN using wavelet analysis [49–52]. In the investigation of inhibitor and surface stability effect in the corrosion process, Liu et al. [52] suggested the use of wavelet standard deviation exponent, which is determined from the slope of log-log plot of standard deviation of wavelet coefficient versus the scales to describe the fractal characteristic of EN signal. They claimed that the wavelet standard deviation exponent describes the corrosion dynamics better than the conventional wavelet exponent [53] and the Hausdorff exponent [9]. More recently, Planinšič and Petek [54] have used the power-law relationship between the variance of wavelet coefficients and scales to extract the fractal dimension of the EN for characterization of the associated corrosion processes. They found that general corrosion can be treated as a stationary random process with weak persistence and pitting corrosion as a non-stationary random process with long-memory, while passivity is modelled as a Brownian motion-like non-stationary

process. A common assumption of fractal approaches is that EN is a homogenous fractal process (monofractal) having the same scaling exponent across all time scales. From the intermittent and bursty non-Gaussian behaviour and the heavy-tailed probability distribution of the fluctuations, EN seems to exhibit inhomogeneous fractal characteristics with non-linear exponents for  $q$ th order structure functions or with time-dependent scaling exponents. One possible interpretation of this inhomogeneity in a fractal process can be attributed to multifractality, which can be thought of as a complex set of interwoven scaling subsets that cannot be described by single exponent like the fractal dimension or the Hurst exponent [10,11].

In this study, we first demonstrate that EN is not a homogeneous fractal signal by using wavelet scalogram analysis. The multifractality of EN is then examined using Legendre spectrum (LS) and large deviation spectrum (LDS). We propose the application of a multiplicative multifractal wavelet model (MWM) to describe the general multifractal characteristics of EN. MWM was developed by Riedi et al. [11] for the modelling of network traffic. Likewise, it is assumed here that the EN is generated by a multiplicative cascade process with long-range dependence. At the microscopic time scale, the EN may be viewed as the result of aggregation of a large number of independent individual sources switching between 'ON' and 'OFF' states. The empirical data used in this study are obtained from zero-resistance ammeter (ZRA) measurement of EN signals of ASTM A106 carbon steel specimens undergoing corrosion in distilled water at room temperature.

#### 4. Corrosion experiment

Two cylindrical electrodes made from A106 mild steel (wt.%: C 0.35, Mn 0.29–1.06, P 0.025, S 0.025, Si 0.1 and Fe remaining) with  $0.8 \text{ cm}^2$  surface area are embedded inside a resin filled cylindrical probe. An electrochemical cell is formed together with an addition Ag/AgCl reference electrode cell with saturated KCl as filling solution. The exposed surfaces of both working electrodes are first abraded with emery paper (1500 grade) and polished with deagglomerated alumina. The polished surfaces are rinsed with distilled water and acetone. The electrode probe is then connected to the potentiostat and active surface is immersed in a cell filled with distilled water and maintained at room temperature ( $27^\circ\text{C}$ ). EN data are recorded using Gamry Ref600 zero-resistance ammeter (ZRA) with three-electrode configuration. The data sampling frequency is set at 1 Hz and the recording is done for duration of 24 h. From the continuous electrochemical noise time series, we arbitrarily choose four temporal regimes for the potential and current fluctuation signals, namely at 0–2 h, 4–6 h, 10–12 h and 20–22 h to study the multifractal characteristics of EN. The regimes are loosely chosen as to capture different stages of the corrosion. At the first hour, the corrosion rate appeared to be very slow, while at the last hours, the top surface of the sample is completely covered with oxide layer. The morphologies of the carefully cleaned surfaces at these four selected durations are shown in Fig. 1. The bright areas

in the images are the corroded regions. One may also notice dark spots at the centre of these bright areas, which are most likely the pitting sites. Detailed study of the microstructure using SEM and AFM will be reported elsewhere. In this work, we shall confine the analysis to the EN signals. The potential and current noise signals are shown in Fig. 2 and Fig. 3, respectively.

### 5. Theory and methods

#### 5.1. Fractal and multifractal signals

A random process  $X(t)$  is said to be self-similar with the Hurst index  $H (> 0)$  if it satisfies the scale invariance relation  $X(\lambda t) \equiv \lambda^H X(t)$  for any  $\lambda > 0$ , (where  $\equiv$  stands for equality in the sense of distribution for a fixed  $t$  and  $\lambda$ ) [9,46]. This implies that the sample paths  $(t, X)$  and  $(\lambda t, (1/\lambda)^H X)$  are statistically equivalent to each other.

One of the most quoted examples of Gaussian self-similar processes with stationary increments is the fractional Brownian motion (FBM) [46] indexed by  $H \in [0, 1]$ . The increment processes of FBM are associated with the fractional Gaussian noise (FGN) that exhibits interesting behaviour at different regimes of the Hurst exponents. FGN is said to be anti-persistent or exhibiting short-memory (analogous to the notion of sub-diffusion in transport phenomena) for  $0 < H < 0.5$ , while  $0.5 < H < 1$  refers to persistent or long-memory (or super-diffusion). FBM reduces to the standard Brownian motion when  $H = 0.5$  with the increment processes corresponding to the uncorrelated Gaussian white noise. The stationary increment property together with self-similarity allows one to define power spectral density with power-law behaviour  $S(f) \sim |f|^{-\beta}$ , where  $\beta = 2H + 1$  is the spectral exponent mentioned earlier [55]. Even though the FBM and FGN have been very successful in the modelling of monofractal processes with a single Hurst exponent or fractal dimension, they are not suitable for scaling phenomena with non-Gaussian behaviour or transient processes with complicated local scaling features.

A generalization of the monofractal concepts is provided by multifractal analysis [10]. A process  $X(t)$  is said to be a multifractal if it has stationary increments and the  $q$ th order moment of  $X(t)$  satisfies  $E[|X(t)|^q] = b(q)^{\tau(q)+1}$ , where  $\tau(q)$  is called the scaling function or generalized Hurst exponent of the multifractal process. Monofractal is a degenerative case of the multifractal process with scaling function  $\tau(q) = qH - 1$ , where  $H$  is the Hurst exponent. The Legendre spectrum  $f_L := \tau^*(\alpha)$  is obtained from the Legendre transform of the scaling function. Let us recall the definition of the local Hölder exponent of a function or distribution  $f$  at point  $t_0$ . Assuming there exists a constant  $C$  and a polynomial  $P_n(t)$  of order  $n$  such that  $t$  is in a neighbourhood of  $t_0$ , one then has  $|f(t) - P_n(t - t_0)| \leq C|t - t_0|^\alpha$ , where  $\alpha$  is the local Hölder exponent. The Hölder exponent quantifies the scaling properties of a process at point  $t_0$  such that the lower values correspond to the more irregular variations. A multifractal process can be considered as a continuum of fluctuations of diverse local scales, and this feature is

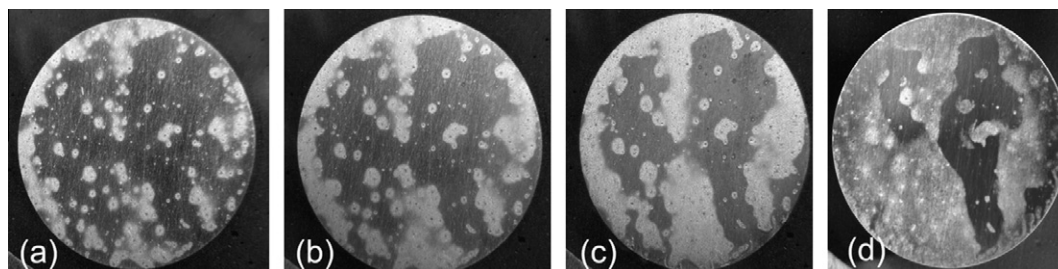


Fig. 1. Morphologies of corroded surface at (a) 0–2 h, (b) 4–6 h, (c) 10–12 h and (d) 20–22 h.

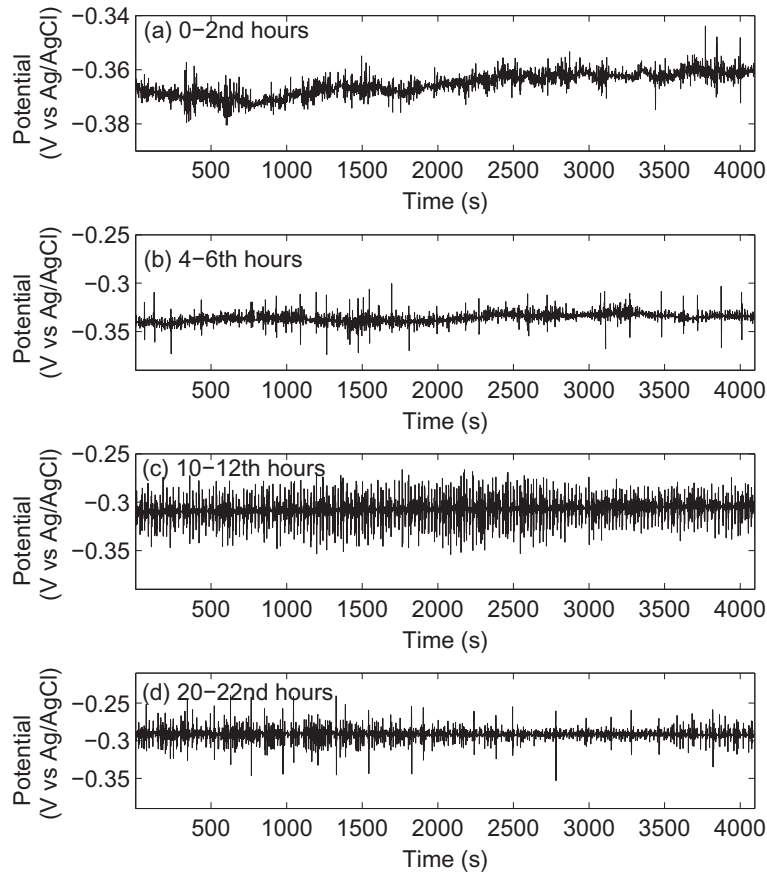


Fig. 2. Electrochemical potential signals at different temporal stages of corrosion: (a) 0–2 h, (b) 4–6 h, (c) 10–12 h and (d) 20–22 h.

characterized by the smooth Legendre spectrum which represents the distribution of Hölder exponents.

Another way to obtain the multifractal spectrum is through the large deviation spectrum derived from Cramèr's theorem of large deviations [56,57]. This definition offers a good compromise between accuracy and computational complexity. The large deviation spectrum is defined as

$$f_g(\alpha) = \lim_{\varepsilon \rightarrow 0} \lim_{n \rightarrow \infty} \frac{\ln N_\varepsilon^n(\alpha)}{-\ln \delta_n}, \quad (1)$$

where

$$N_\varepsilon^n(\alpha) = \#\{\alpha_i^n \mid |\alpha - \alpha_i^n| < \varepsilon\}. \quad (2)$$

$N_\varepsilon^n(\alpha)$  denotes the number of intervals having a coarse grain Hölder exponent  $\alpha_i^n$ , close to a Hölder exponent  $\alpha$  up to a precision  $\varepsilon$ . The term in the denominator  $\delta_n$  is related to the partition defined by the measure at  $n$ th resolution. The  $f_g(\alpha)$  spectrum is then estimated using a kernel-density-based method [58]. Contrary to the Legendre spectrum of a multifractal process which is a concave function, the large deviation spectrum does not need to be concave, thereby is more appropriate in a general setting. The multifractal formalism essentially holds for both singularity spectra, but  $f_g$  contain more information than  $f_L$ . It can be proven that  $f_L$  is the concave hull of  $f_g$ , thus  $f_g(\alpha) \leq f_L(\alpha)$  [59].

## 5.2. Wavelet scalogram

In our work, we use the discrete wavelet transform for multi-scale analysis of EN. According to the theory of multiresolution analysis, a discrete sequence  $X(t)$  of length  $N = 2^j$  can be represented in terms of orthogonal bases ( $\varphi_{j,k}(t) = 2^{j/2} \varphi(2^j t - k)$ ,

$\psi_{j,k}(t) = 2^{j/2} \psi(2^j t - k)$ ) constructed from dilation and shift operation of the father scaling function  $\varphi(t)$  and mother wavelet  $\psi(t)$  [60]. Thus, one can write the multiscale decomposition of  $X(t)$  as

$$X(t) = \sum_{k=0}^{2^j-1} U_{j_0,k} \varphi_{j_0,k}(t) + \sum_{j=j_0}^J \sum_{k=0}^{2^j-1} W_{j,k} \psi_{j,k}(t), \quad (3)$$

where the scaling coarse coefficients  $U_{j,k}$  and the wavelet detail coefficients  $W_{j,k}$  at particular scale index  $j$  and position index  $k$  are given by

$$U_{j,k} := \int X(t) \varphi_{j,k}(t) dt, \quad (4)$$

and

$$W_{j,k} := \int X(t) \psi_{j,k}(t) dt, \quad (5)$$

respectively. The  $q$ th order scalogram at scale  $j$  is then given by

$$S_q(j) = \frac{1}{N_j} \sum_{k=0}^{2^j-1} |W_{j,k}|^q, \quad (6)$$

where  $N_j$  is the length of the detail coefficient vector used to normalize the generalized 'wavelet energy'. If  $X(t)$  is scaling signal, then  $S_q(j)$  obeys a power-law relation

$$S_q(j) \sim (2^{-j})^{\zeta(q,H)} \quad (7)$$

For a homogeneous fractal signal (i.e. monofractal),  $\zeta(q,H) = qH$  and the scaling exponent (or Hurst exponent) can be determined from the slope of  $\log_2 S_q(j)$  versus  $j$  plot. On the contrary,  $\zeta(q,H)$  exhibits a complex non-linear dependence on  $q$  for inhomogeneous

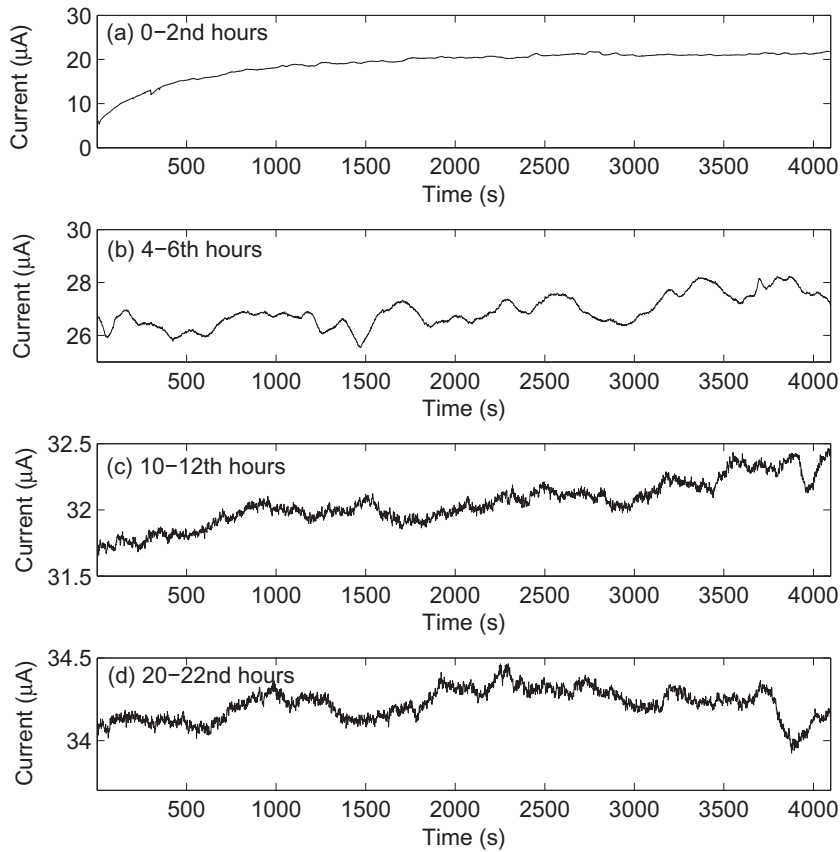


Fig. 3. Electrochemical current signals at different temporal stages of corrosion: (a) 0–2 h, (b) 4–6 h, (c) 10–12 h and (d) 20–22 h.

scaling or multifractal signals. The  $q$ th order wavelet scalogram will be used to justify the non-uniform in the scaling behaviour of the EN signals.

### 5.3. Wavelet transform modulus maxima method

The wavelet transform modulus maxima (WTMM) method [10] is used in this study to estimate the empirical multifractal spectrum of EN. By choosing an appropriate wavelet  $\psi$ , one can eliminate the polynomial behaviour of a function, so as to analyze its regularity. If the first  $(n + 1)$  moments of  $\psi$  are zero, then it is known that the wavelet transform of  $X$  denoted as  $T_\psi[X](t_0, a_0^j)$  scales as  $(a_0^j)^{h(t_0)}$  [10]. Thus, the local singular behaviour of  $X$  around  $t_0$  is characterized by a power-law scaling exponent  $h(t_0)$  of the wavelet transform of  $X$  at the point  $t_0$  when the scale  $a_0^j$  goes to 0. The WTMM method can be considered as the generalization of classical box-counting technique. The key feature of this method is the scaling behaviour of partition function defined in terms of wavelet coefficients,

$$Z(q, a_0^j) = \sum_{i \in L(a_0^j)} \left[ \sup_{(t, a_0^i) \in I} |T_\psi[X](t, a_0^i)| \right]^q \sim (a_0^j)^{\tau(q)}, \quad (8)$$

where  $q \in \mathbb{R}$ . The sum is taken over the wavelet transform' skeleton defined at each scale  $a_0^j$  by the local maxima of  $|T_\psi[X](t, a_0^j)|$ . There WTMM are disposed on connected curves called maxima lines and the set of  $L(a_0^j)$  of all maxima lines that exist at scale  $a_0^j$  indicates how to position the wavelets in order to obtain a partition at this scale. The scaling exponent  $\tau(q)$  is obtained from the slope of log partition function versus log scale. The singularity spectrum  $f_L(\alpha)$  is then obtained by Legendre transform of  $\tau(q)$ , namely  $f_L(\alpha) = \min(q\alpha - \tau(q))$ . Homogeneous fractal functions are characterized by a linear  $\tau(q)$  spectrum (i.e. function with constant Hölder

exponent). On the contrary, a non-linear  $\tau(q)$  spectrum implies multifractal properties (i.e. function with fluctuating Hölder exponents). For certain values of  $q$ ,  $\tau(q)$  have some well-known interpretations. For example,  $\tau(0)$  can be identified as the fractal dimension (capacity) of the set where  $X$  is not smooth,  $\tau(1)$  is related to the capacity of the graph of the function and  $\tau(2)$  is related to the scaling exponent  $\beta$  of spectral density  $\Gamma_B(f) \propto |f|^{-\beta}$ , with  $\beta = 2 + \tau(2)$ . One can related this property to the presence of long-range correlation in the time series.

### 5.4. Multifractal wavelet model

The multifractal wavelet model (MWM) is a multiplicative cascade model that uses the inherent scaling properties of the wavelet basis to generate a multifractal process. Using this model, one can synthesize a time series that exhibits long-range dependence, having a non-Gaussian probability density function and non-linear scaling of the  $q$ th order structure function.

In the MWM construction, one starts from the coarsest scale coefficient,  $U_{J_0,0}$  which is then multiplied by a random multipliers  $A_{j,k}$  with constraint such that the detail coefficient  $W_{j,k}$  is given by  $W_{j,k} = A_{j,k}U_{j,k}$  for  $k = 0, \dots, 2^j - 1$  [11]. The scale coefficient for the next scale is calculated through iteration rules:  $U_{j+1,2k} = 2^{-1/2}(U_{j,k} + W_{j,k})$  and  $U_{j+1,2k+1} = 2^{-1/2}(U_{j,k} - W_{j,k})$ . The iterative process is repeated until the finest scale  $j = J$ . The output of MWM is the finest-scale coefficients,  $C^{(j)}[k] = 2^{-j/2}U_{j,k}$ ,  $k = 0, \dots, 2^j - 1$ . The random multipliers  $A_{j,k}$  are independent random variables symmetrically distributed over  $(-1, 1)$  and generated from beta distribution with a probability density function given by [61]

$$g(A) = \frac{(1+A)^{p-1}(1-A)^{p-1}}{\beta(p,p)2^{2p-1}}, \quad (9)$$

where  $\beta(p, p)$  is the beta function and  $p > 0$  is the beta parameter used to control the scaling behaviour of wavelet coefficient. The beta distribution will approach the Gaussian distribution for large  $p$  [61]. In addition, the variance of the beta random variable follows  $E[A^2] = 1/(2p + 1)$ . In MWM, the long-range dependence of the output signal is controlled by behaviour of the wavelet energy decays across the scales. The ratio of wavelet energy between scale,  $\eta_j$  is parameterized via the variance of multipliers

$$\eta_j = \frac{E[W_{j-1,k}^2]}{E[W_{j,k}^2]} = 2 \frac{E[A_{(j-1)}^2]}{E[A_{(j)}^2] (1 + E[A_{(j-1)}^2])}. \tag{10}$$

The variance of multipliers at coarsest scale  $J_0$  is obtained through

$$E[A_{(J_0)}^2] = \frac{E[W_{J_0,k}^2]}{E[U_{J_0,k}^2]}. \tag{11}$$

The higher-order moments and marginal probability density function of the output signal is controlled through the moments of scaling coefficient [11]

$$\frac{E[U_{j-1,k}^q]}{E[U_{j,k}^q]} = 2^{q/2} E[(1 + A_{(j-1)})^q]^{-1}. \tag{12}$$

In order to fit the MWM to the electrochemical data, the variances of wavelet coefficients  $E[W_{j,k}^2]$ ,  $j = J_0, \dots, J - 1$  and of coarsest scale coefficients,  $E[U_{J_0,k}^2]$  are calculated from the EN signals using Haar wavelet transform.

## 6. Results and discussions

### 6.1. Wavelet scalogram analysis

The wavelet energy scalogram  $S_q(j)$  of EN signal as given in (6) is calculated using Daubechies wavelet for 12 scale levels and moment orders,  $q = 1, 2, 3, 4, 5$ . The results are plotted in Fig. 4 and Fig. 5 for potential and current signals, respectively. It can be seen that the wavelet scalogram for potential signals deviates from linear scaling for almost all values of  $q$ , indicating an inhomogeneous fractal property. Meanwhile, for the current signals, deviations from linear scaling in the scalograms are only apparent for higher orders of  $q$ , suggesting less complexity in the fractal behaviour compared to potential signals. The qualitative features of the scalograms do appear to show minor changes between different temporal regimes of the corrosion process at higher orders of  $q$ . In general, an inhomogeneous fractal property indicates the possibility of multifractal structure in the EN. This observation is verified in the next section using multifractal analysis.

### 6.2. Multifractal Legendre spectrum and large deviation spectrum

Estimation of multifractal spectra is carried using a Matlab-based FracLab toolbox developed by INRIA (<http://fractales.inria.fr>). For the Legendre spectrum estimation, we use the Daubechies D8 analyzing wavelet for the multiscale decomposition of the signals up to 12 scale levels. The  $q$  exponents in the partition function vary from  $-10$  to  $10$  with  $0.5$  increment. Meanwhile, for the large deviation spectrum estimation, the coarse grain Hölder exponent is calculated in single resolution. The oscillation mode was chosen to measure the variation of the signal in each interval to determine its scaling behaviour. In the actual computation of the

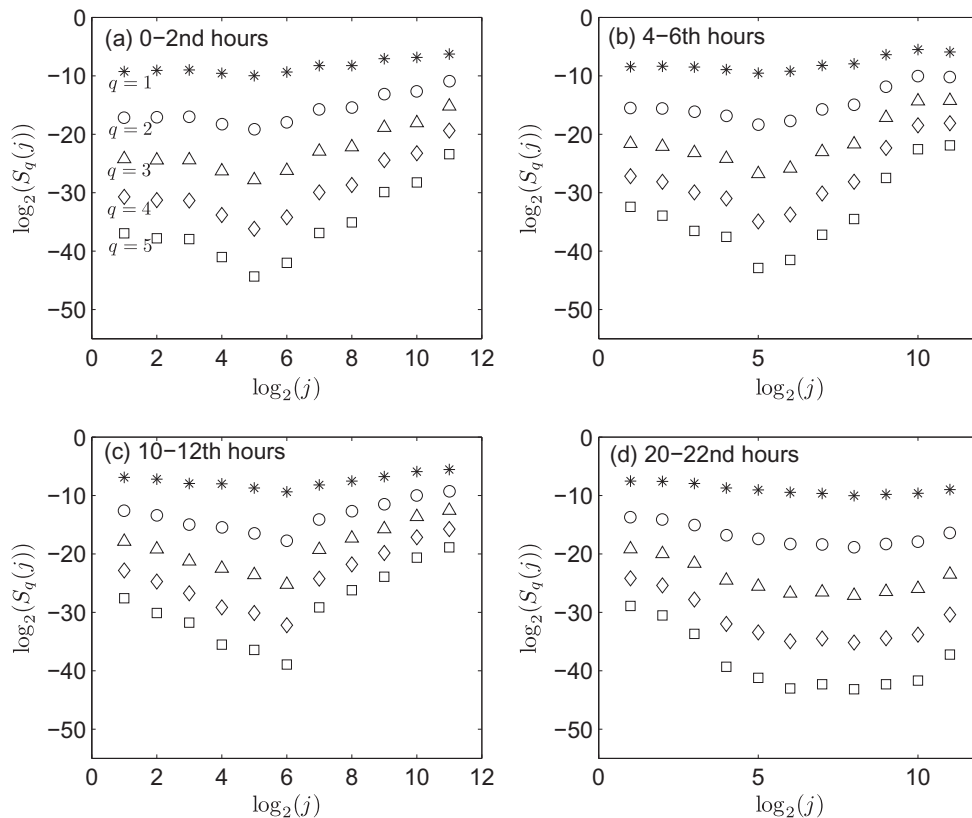


Fig. 4. Wavelet scalogram of EN potential signals at different temporal stages of corrosion.

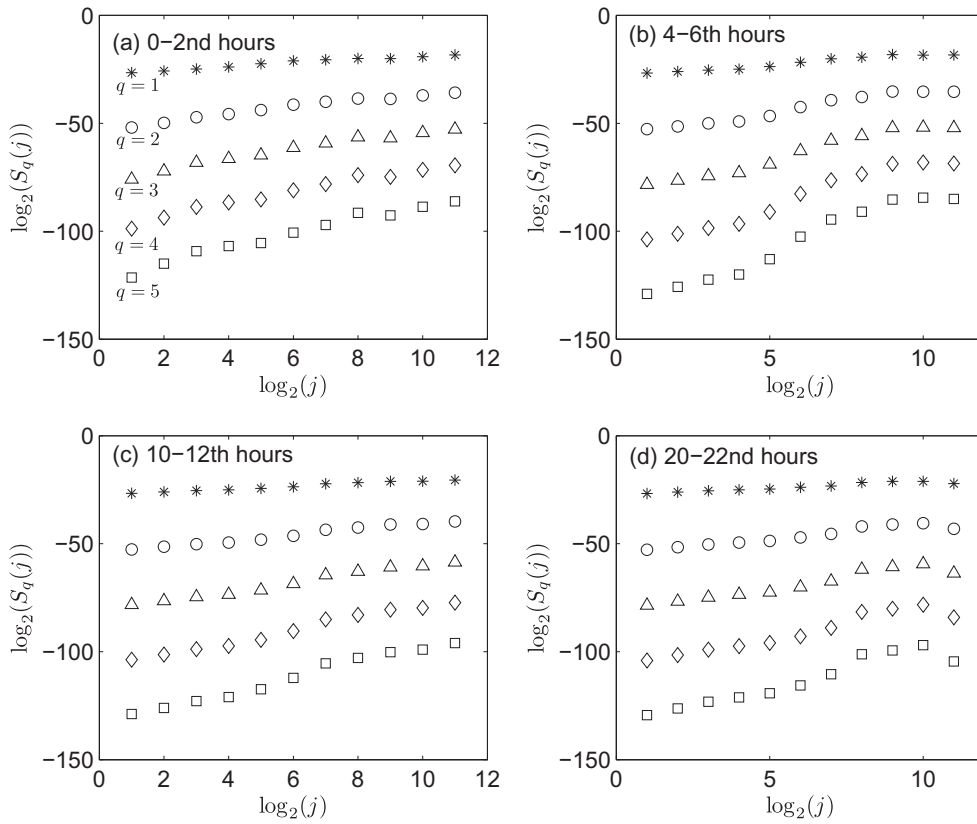


Fig. 5. Wavelet scalogram of EN current signals at different temporal stages of corrosion.

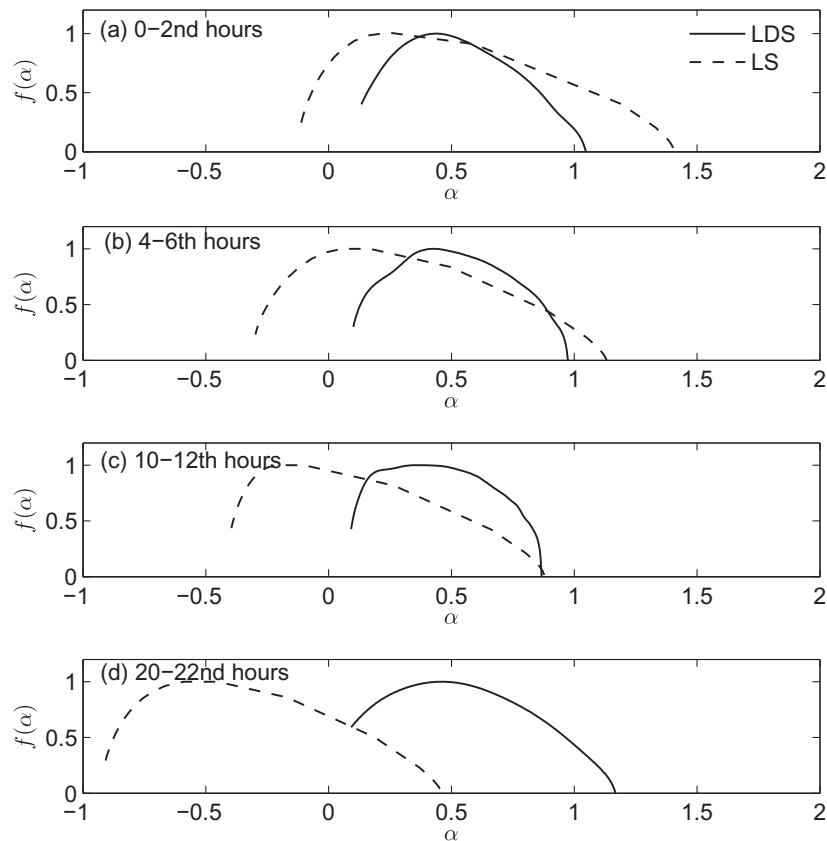


Fig. 6. Empirical multifractal large deviation spectra (solid line) and Legendre spectra (dashed line) for EN potential signals at different temporal stages of corrosion.

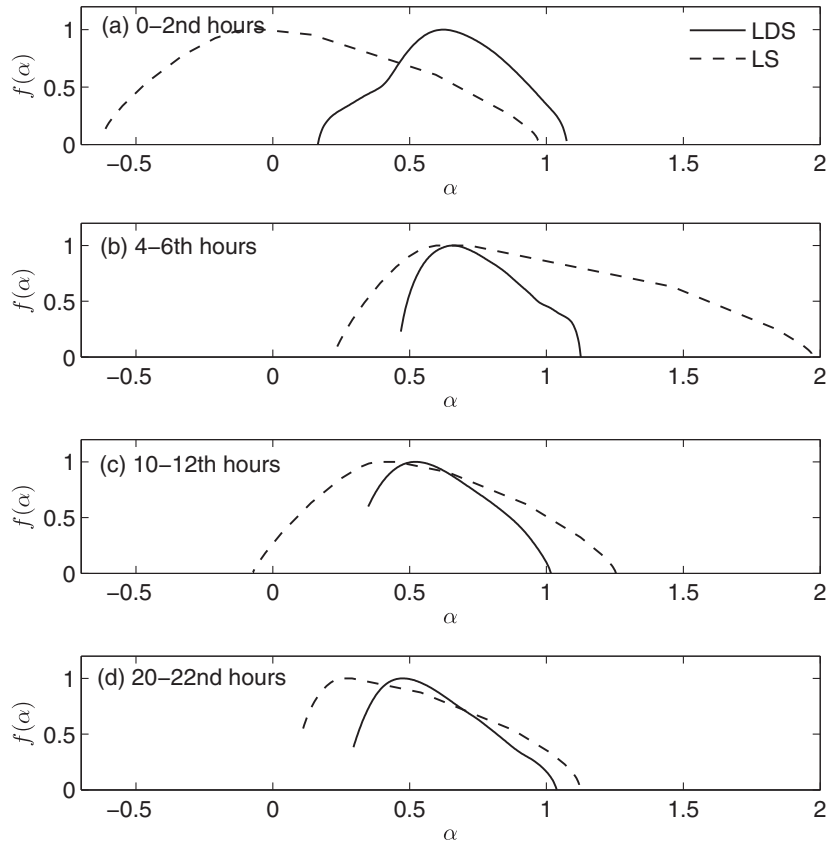


Fig. 7. Empirical multifractal large deviation spectra (solid line) and Legendre spectra (dashed line) for EN current signals at different temporal stages of corrosion.

large deviation spectrum, continuous density of the coarse grain exponents were estimated using Gaussian kernel with optimal size computed from some empirical statistical criteria. The multifractal spectra using both estimations are shown in Fig. 6 for potential signals and Fig. 7 for current signals. The main parameters of the empirical multifractal singularity distribution namely the most likely Hölder exponents  $\alpha_0$  and the range of Hölder exponents,  $\Delta\alpha = |\alpha_{max} - \alpha_{min}|$  are summarized in Table 1.

As for EN potential signals, both the Legendre spectrum and large deviation spectrum show a broad range of singularity values. It means that the fluctuations of potential signals are multifractal. In the case of current signals, both the Legendre spectrum and

large deviation spectrum show a relatively narrower range of singularity values compared to the potential signals. The results from Legendre spectrum and large deviation spectrum strongly suggest the occurrence of multifractal behaviour in the corrosion processes. The potential signals are found to exhibit more obvious signatures of multifractality, as can be visually seen from spikiness of the fluctuations in the signals. A temporal dynamics of the multifractal statistics is also noticeable in current and potential signals observed at different stages of corrosion. From the asymmetrical shape of the multifractal spectra, one may note that non-trivial multiplicative structures may possibly exist in corrosion mechanisms. Superposition of more than one measure with disjointed support and phase transition can be attributed as the cause of non-concavity of the multifractal spectrum [59]. In the next section, we attempt to simulate EN signals by multiplicative cascade processes using parameterized beta distribution and wavelet coefficients.

Table 1  
Hölder exponents of multifractal Legendre spectrum (LS) and large deviation spectrum (LDS) for empirical (e) and simulated (s) EN signals.

Signals	$\alpha_{oLS}$	$\Delta\alpha_{LS}$	$\alpha_{oLDS}$	$\Delta\alpha_{LDS}$
$V_{T1,e}$	0.25	1.52	0.44	0.91
$V_{T1,s}$	0.18	1.13	0.36	0.67
$V_{T2,e}$	0.05	1.43	0.43	0.87
$V_{T2,s}$	-0.04	1.29	0.31	0.62
$V_{T3,e}$	-0.20	1.27	0.40	0.78
$V_{T3,s}$	-0.35	1.06	0.28	0.72
$V_{T4,e}$	-0.57	1.36	0.48	1.08
$V_{T4,s}$	-0.50	1.30	0.27	0.60
$I_{T1,e}$	-0.06	1.58	0.63	0.91
$I_{T1,s}$	-0.18	1.17	0.46	0.79
$I_{T2,e}$	0.60	1.75	0.67	0.66
$I_{T2,s}$	0.34	1.52	0.60	0.99
$I_{T3,e}$	0.40	1.32	0.52	0.67
$I_{T3,s}$	0.34	1.20	0.47	0.73
$I_{T4,e}$	0.25	1.02	0.48	0.74
$I_{T4,s}$	0.25	1.08	0.45	0.93

### 6.3. Multifractal wavelet modelling of electrochemical noise

In order to simulate the fluctuation with a similar multifractal structure, we determine the variance of wavelet coefficients, mean and variances of the scaling function coefficients at the coarsest level. The  $p$ -parameter of the symmetric beta distribution is determined from the variance of the multipliers  $A(j, k)$  which is related to the ratio of the variances of wavelet energy at two successive levels. The calculation is initialized at where the variance of multipliers is equal to the ratio of wavelet energy and variance of scaling coefficient at the coarsest scale ( $J_0 = 4$ ). The values of  $p$  at nine scales (i.e.  $j = 4, \dots, 12$ ) of the wavelet coefficients for potential and current signals are summarized in Table 2. The sample paths of the simulated potential and current time series are shown

**Table 2**  
Parameter  $p$  for symmetric beta distribution at wavelet scale  $j$  for simulating potential and current signals.

Signal	Parameter $p$ ( $\times 10^6$ ) at wavelet scale									
	$j = 4$	5	6	7	8	9	10	11	12	
$V_{T1,e}$	0.217	0.297	0.247	0.463	0.595	0.377	0.130	0.625	0.349	
$V_{T2,e}$	0.064	0.174	0.281	0.370	0.254	0.084	0.026	0.008	0.004	
$V_{T3,e}$	0.698	1.304	0.673	0.297	0.096	0.020	0.008	0.002	0.001	
$V_{T4,e}$	1.309	1.079	0.946	0.318	0.100	0.035	0.009	0.002	0.001	
$I_{T1,e}$	0.798	0.055	0.031	0.053	0.124	0.310	0.507	1.432	2.571	
$I_{T2,e}$	0.010	0.013	0.026	0.055	0.181	0.542	1.476	2.681	3.897	
$I_{T3,e}$	0.521	0.699	0.710	1.471	3.356	4.494	5.444	5.150	5.991	
$I_{T4,e}$	0.283	0.573	1.055	2.195	4.574	6.589	7.163	7.110	8.003	

in Fig. 8. The multifractal Legendre and large deviation spectra of the synthesized signals are determined and compared with the empirical multifractal spectra (see Table 1). Figs. 9 and 10 show the empirical and simulated multifractal spectra for potential signals and Figs. 11 and 12 for current signals.

The multifractal spectra of the simulated current signals with  $p$ -parameterized beta distribution for the multiplicative cascade generally fit the empirical singularity range and the most likely (maximum probability) Hölder exponent values. There is, however, one exception, namely the current signal for 4–6 h duration that has shifted by 0.2 to the left. The MWM-based simulated data produce a good fit in upper right parts, which corresponding to  $q < 0$  (slopes of tangents to the Legendre spectrum), indicating good agreement for negative order moments. The chance of observing lower value of Hölder exponents is considerably high, corresponding to slower decay of wavelet energy than the original empirical signals. On the other hand, the MWM is able to capture the positive order moments of the empirical current signals based on the good fit in upper left parts of the spectra. However, the upper right parts of the simulated spectra show lower probability than the original

spectra. This might be due to the relatively slow decay of wavelet energy with negative moment compared to the original current signals.

The physical origin of multifractal structures in EN signals can be interpreted as an aggregation of elementary processes which switch between two states, denoted ‘ON’ and ‘OFF’ states. The ‘ON’ state can be interpreted as the state where there is a pulse of charges produced from the electrochemical reaction and the ‘OFF’ state as a period with a relatively calm or silent state. These elementary events are considered to be independent to each other and randomly distributed across the time scale. Aggregation of these processes with multiplicative cascade across the scales from the finest to the coarsest would generate fluctuation with complex non-linear scaling and long-range dependence. From the point of view of corrosion mechanisms, fluctuation of local conditions (at small scales) on the metal may cause passive layer breakdown and generate a sudden rise in current [62–64]. The metastable state would be reached when the initiated corrosion site may repassivate quickly or grow and then repassivate. Finally, the stable pitting state is reached when the rate of corrosion site dissolu-

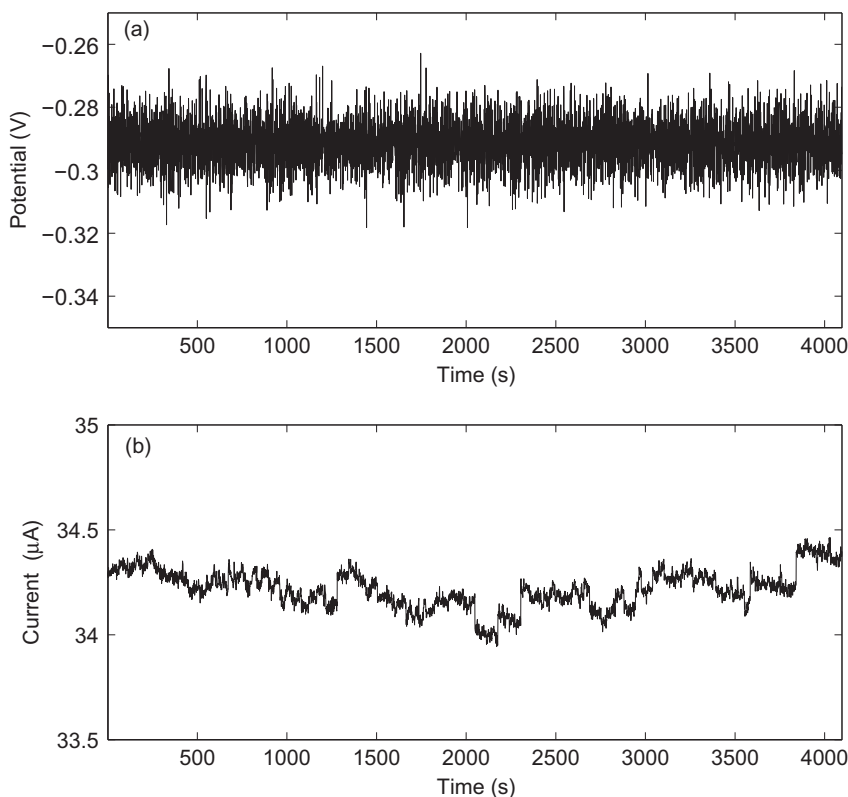


**Fig. 8.** Simulated time series of (a) potential and (b) current signals using multifractal wavelet model.

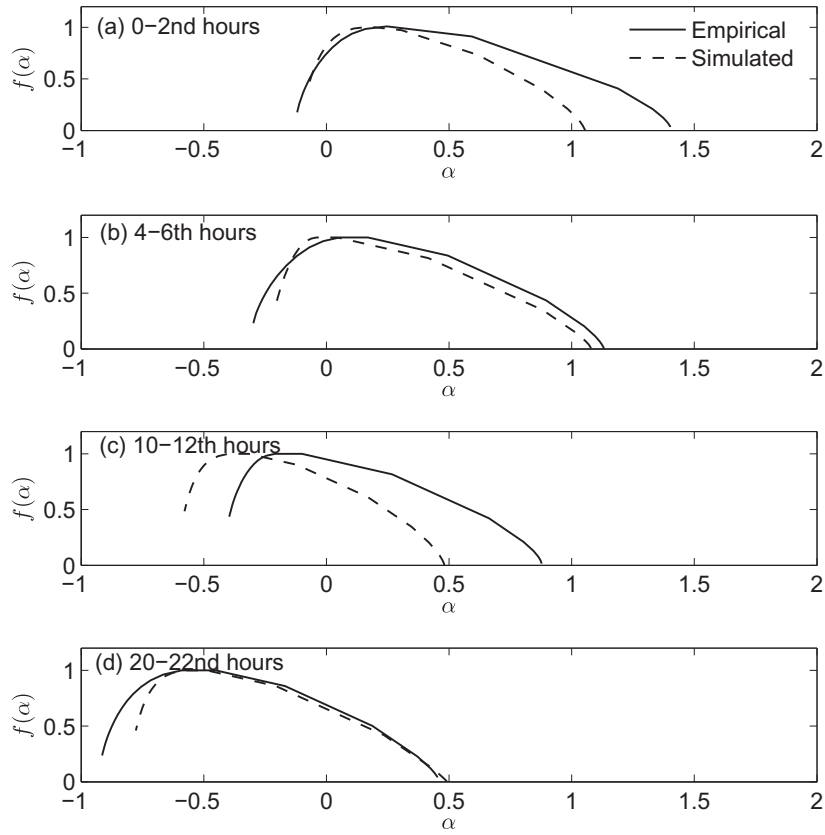


**Fig. 9.** Comparison of Legendre spectra of empirical (solid line) and simulated (dashed line) potential signals.

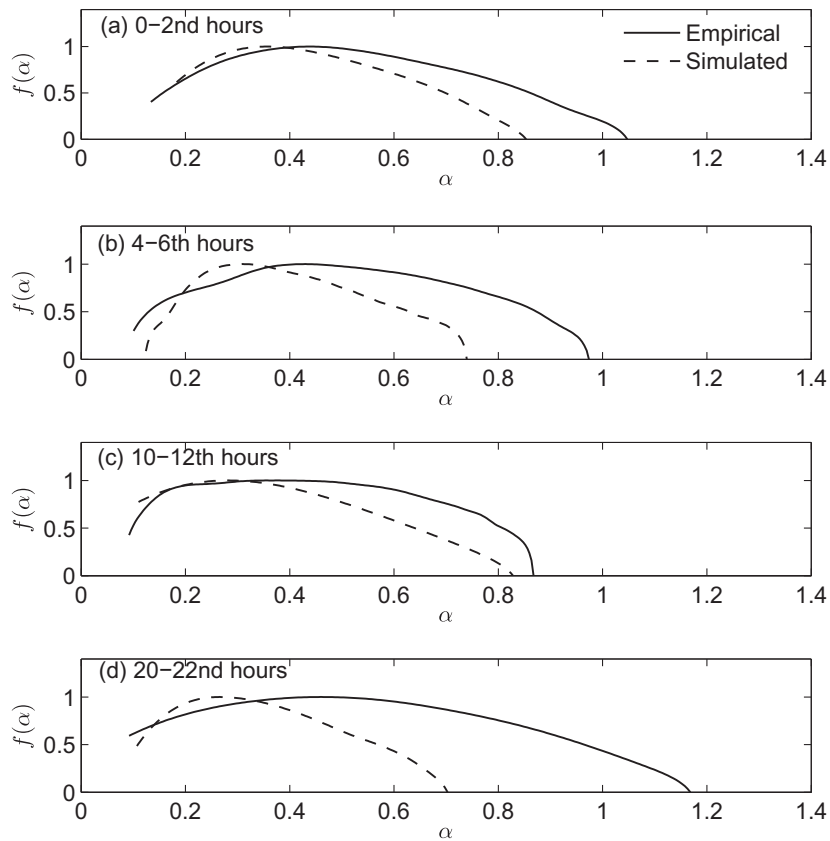


**Fig. 10.** Comparison of large deviation spectra of empirical (solid line) and simulated (dashed line) potential signals.

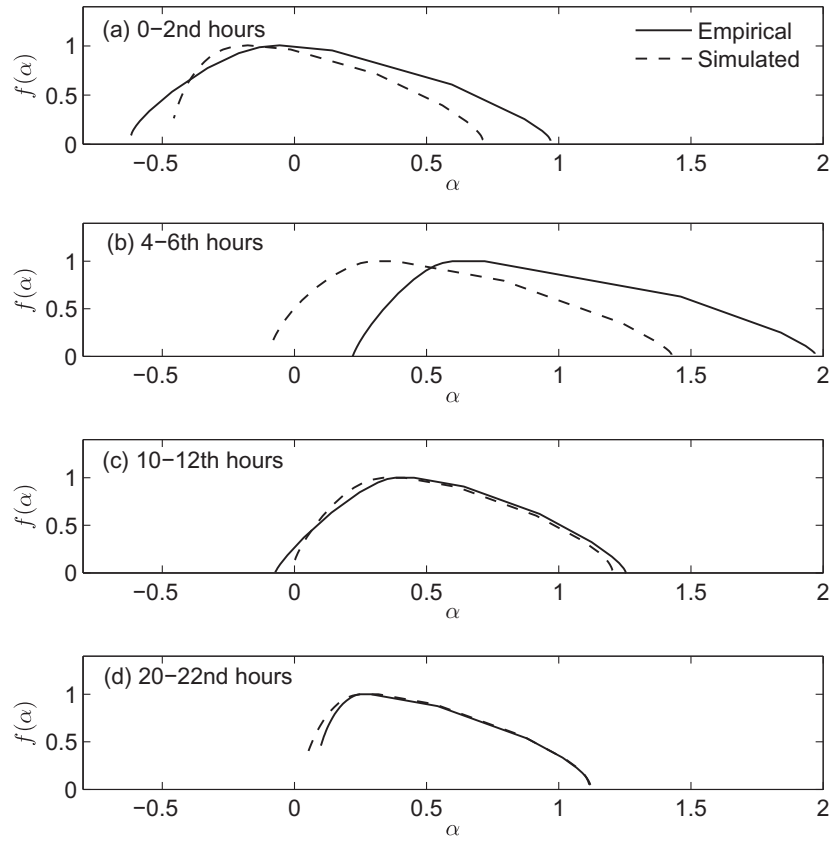


Fig. 11. Comparison of Legendre spectra of empirical (solid line) and simulated (dashed line) current signals.

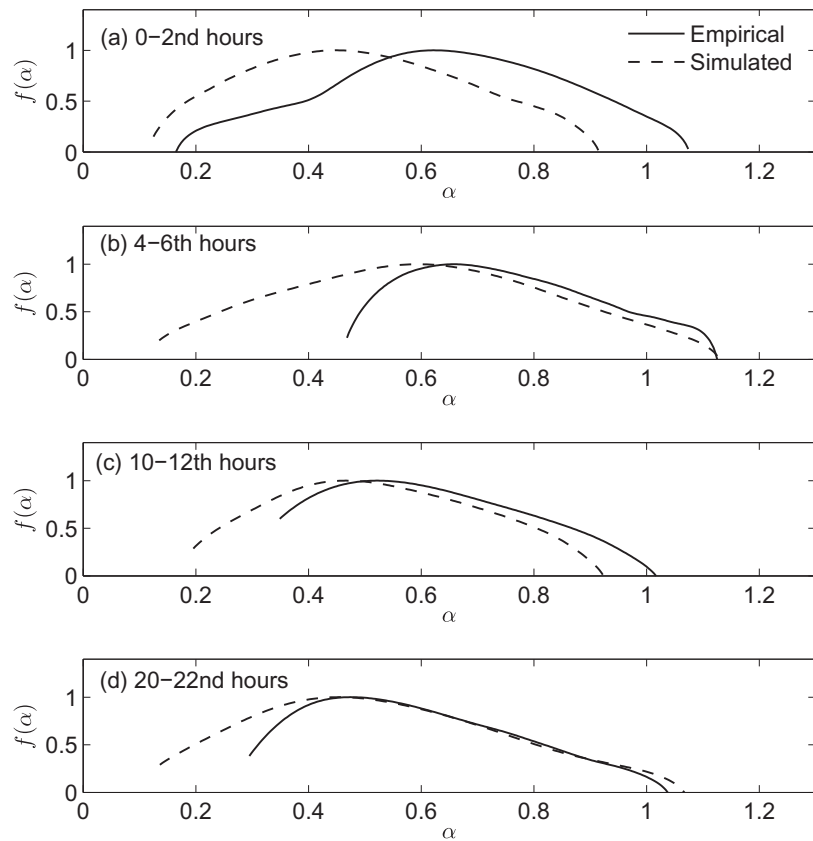


Fig. 12. Comparison of large deviation spectra of empirical (solid line) and simulated (dashed line) current signals.

tion becomes greater than the repassivation rate [29]. Another possible mechanism is related to activation-controlled dissolution, where a sudden burst of charges occurs as the dissolution of ledges is ‘unlocked’ by the first atom within the ledge [65]. Even though initiation of a corrosion site may appear to be random, the corrosion process may acquire long-range dependence and multifractality due to the multiplicative cascade nature of underlying mechanisms.

## 7. Conclusions

The understanding of the origin of potential and current fluctuations in electrochemical noise has been improved over the years due to the availability of novel techniques such as fractal and wavelets analyses. In this study, we have examined the EN time series using a multifractal approach that generalizes the concept of uniform scaling to the more ubiquitous multiscaling characteristics. The  $q$ -order wavelet scalogram analysis showed that the potential signals exhibit complicated non-linear scaling for large  $q$  values as compared to the current signals. Both of the signals are shown to be multifractal using Legendre and large deviation spectra. The multifractal spectra are also found to be qualitatively different for different temporal stages of the corrosion process. For example, the Legendre spectrum captures the burstiness observed in the potential signal with distribution concentrated in the regime of smaller values of Hölder exponents. The potential signals become less volatile as the corrosion progresses. One the other hand, the current signals are found to become more irregular (lower Hölder exponents) as the corrosion progresses. The most probable value of Hölder exponents are shifted towards smaller values.

Finally, we remarked on the results obtained from the multifractal wavelet modelling of the EN signals. We have introduced the parameterized beta distribution for the multiplicative cascade process to capture the multifractal spectra of the empirical EN signals. In all of the simulations, the values of beta distribution parameter  $p$  derived from the variance of the random multipliers  $A(j, k)$  are large ( $p \gg 1$ ), indicating that the underlying mechanism at the coarsest scale can be modelled by Gaussian distribution. However, it is noticed that  $p$  values decrease as the scale goes finer (large  $j$  index) for the potential signals. This indicates a tendency towards non-Gaussianity in the fluctuations at the finest scales. Interestingly, an opposite trend is observed for the current signals. In summary, this study supports the incorporation of multifractal characteristics for corrosion monitoring and modelling applications.

## Acknowledgements

The authors thank University of Malaya for financial support under grant UM-RG062/09AFR and the referee for useful suggestions.

## References

- [1] U.R. Evans, *The Corrosion and Oxidation of Metals: Scientific Principles and Practical Applications*, Edward Arnold Publishers, London, 1960.
- [2] G.J. Bignold, *Corrosion in the power industry*, in: I. Milne, R. Ritchie, B.L. Karihaloo (Eds.), *Comprehensive Structural Integrity*, vol. 1, Elsevier, Oxford, 2003, pp. 193–215.
- [3] R.D. Kane, A new approach to corrosion monitoring, *Chem. Eng.* (2007) 34–41.
- [4] D.A. Eden, D.G. John, J.L. Dawson, *Corrosion Monitoring*, US Patent No. 5139627, 1992.
- [5] D.A. Eden, K. Hladky, D.G. John, J.R. Scully, Electrochemical noise – simultaneous monitoring of potential and current noise signals from corroding electrodes, in: *NACE Corrosion Conference*, 1986, Paper No. 274.
- [6] R.A. Cottis, M.A. Al-Ansari, G. Bagley, A. Pettiti, Electrochemical noise measurements for corrosion studies, *Mater. Sci. Forum* 741 (1998) 289–292.
- [7] J.R. Kearns, J.R. Scully, P.R. Roberge, D.L. Reichert, J.L. Dawson (Eds.), *Electrochemical Noise Measurement for Corrosion Applications*, American Society for Testing and Materials, West Conshohocken, 1996.
- [8] S. Mallat, *A Wavelet Tour of Signal Processing*, Academic Press, New York, 1998.
- [9] B.B. Mandelbrot, *The Fractal Geometry of Nature*, W.H. Freeman, San Francisco, 1982.
- [10] J.F. Muzy, E. Bacry, A. Arneodo, Multifractal formalism for fractal signals, *Phys. Rev. E* 47 (1993) 875–884.
- [11] R. Riedi, M. Crouse, V. Ribeiro, R. Baraniuk, A multifractal wavelet model with application to TCP network traffic, *IEEE Trans. Inf. Theory* 45 (1999) 992–1018.
- [12] Z. Szklarska-Smialowska, M. Janik-Czachor, The analysis of electrochemical methods for determination of characteristic potentials of pitting corrosion, *Corros. Sci.* 11 (1971) 901–914.
- [13] K. Hladky, J.L. Dawson, The measurement of localized corrosion using electrochemical noise, *Corros. Sci.* 21 (1981) 317–322.
- [14] J.F. Chen, W.F. Bogaerts, The physical meaning of noise resistance, *Corros. Sci.* 37 (1995) 1839–1842.
- [15] U. Bertocci, F. Huet, Noise analysis applied to electrochemical systems, *Corrosion* 51 (1995) 131–145.
- [16] A. Petek, V. Doleček, V. Vlady, Stochastic analysis of current fluctuations during general corrosion of stainless steel in sulphuric acid, *Corrosion* 53 (1997) 928–934.
- [17] U. Bertocci, C. Gabrielli, F. Huet, M. Keddam, P. Rousseau, Noise resistance applied to corrosion measurements, *J. Electrochem. Soc.* 144 (1997) 31–37.
- [18] P.R. Roberge, R.D. Klassen, M.A.A. Tullmin, Electrochemical noise analysis for corrosive assessment, in: *NACE Corrosion Conference*, 2000, Paper No. 00281.
- [19] J. Goellner, Electrochemical noise for corrosion, *Mater. Corros.* 55 (2004) 727–734.
- [20] A. Heyn, J. Goellner, M. Bierwirth, H. Klapper, Recent application of electrochemical noise for corrosion testing – benefits and restrictions, in: *NACE Corrosion*, 2007, Paper No. 07459.
- [21] Y.J. Tan, S. Bailey, B. Kinsella, A. Lowe, Mapping corrosion kinetics using the wire beam electrode in conjunction with electrochemical noise resistance measurements, *J. Electrochem. Soc.* 147 (2000) 530–539.
- [22] A. Legat, C. Zevnik, The electrochemical noise of mild and stainless steel in various water solutions, *Corros. Sci.* 35 (1993) 1661–1666.
- [23] J.L. Crolet, Mechanisms of uniform corrosion under corrosion deposits, *J. Mater. Sci.* 28 (1993) 2589–2606.
- [24] J.M. Smulko, K. Darowicki, A. Zielinski, On electrochemical noise analysis for monitoring of uniform corrosion rate, *IEEE Trans. Instrum. Meas.* 56 (2007) 2018–2023.
- [25] A. Legat, Influence of electrolyte movement on measure electrochemical noise, *Corrosion* 56 (2000) 1086–1092.
- [26] A. Heyn, J. Goellner, Using electrochemical noise for corrosion testing: determination of critical pitting temperatures, *Mater. Corros.* 58 (2007) 953–960.
- [27] H.S. Klapper, J. Goellner, A. Heyn, The influence of the cathodic process on the interpretation of electrochemical noise signals arising from pitting corrosion of stainless steels, *Corros. Sci.* 52 (2010) 1362–1372.
- [28] G.T. Burstein, S.P. Mattin, Repetitive nucleation of corrosion pits on stainless steel and the effects of surface roughness, *J. Electrochem. Soc.* 148 (2001) B504–B516.
- [29] G.T. Burstein, C. Liu, R.M. Souto, S.P. Vines, Origins of pitting corrosion, *Corros. Eng. Sci. Technol.* 39 (2004) 25–30.
- [30] H.H. Uhling, R.W. Revie, *Corrosion and Corrosion Control*, third ed., Wiley, New York, 1985.
- [31] E. Osarolube, I.O. Owate, N.C. Oforka, Corrosion behaviour of mild and high carbon steels in various acidic media, *Sci. Res. Essay* 3 (2008) 224–228.
- [32] S. Arzola-Peralta, J. Genesca Llongueras, M. Palomar-Pardave, M. Romero-Romo, Study of the electrochemical behaviour of a carbon steel electrode in sodium sulphate aqueous solutions using electrochemical impedance spectroscopy, *J. Solid State Electrochem.* 7 (2003) 283–288.
- [33] G. Bikulchuy, A. Ruchinskene, V. Deninis, Corrosion behavior of low-carbon steel in tap water treated with permanent magnetic field, *Prot. Met.* 39 (2003) 443–447.
- [34] A. Hemmasian-Ettefagh, M. Amiri, C. Dehghanian, Corrosion inhibition of carbon steel in cooling water, *NACE Int.* 49 (2010) 60–65.
- [35] K. Matsunami, T. Kato, K. Sugimoto, Corrosion of carbon steel and its estimation in aqueous solution used in petroleum refineries, *Int. J. Press. Vessels Pip.* 45 (1991) 179–197.
- [36] A. Nagiub, F. Mansfeld, Evaluation of microbiologically influenced corrosion inhibition using electrochemical noise analysis, *Corros. Sci.* 43 (2001) 2001–2009.
- [37] O. Lahodny-Sarc, F. Kapor, Corrosion inhibition of carbon steel in the near neutral media by blends of tannin and calcium gluconate, *Mater. Corros.* 53 (2002) 264–268.
- [38] E. Sarmiento, J.G. Gonzales-Rodriguez, J. Uruchurtu, A study of the corrosion inhibition of carbon steel in a bromide solution using fractal analysis, *Surf. Coat. Technol.* 184 (2004) 322.
- [39] A.M. Badiea, K.N. Mohana, Corrosion mechanism of low-carbon steel in industrial water and adsorption thermodynamics in the presence of some plant extracts, *J. Mater. Eng. Perform.* 18 (2009) 1264–1271.
- [40] C. Wang, Z.Y. Wang, W. Ke, The effect of environment variables on atmospheric corrosion of carbon steel in Shenyang, *Chin. Sci. Bull.* 54 (2009) 3438–3445.
- [41] K. Hladky, J.L. Dawson, The measurement of corrosion using electrochemical  $1/f$  noise, *Corros. Sci.* 22 (1982) 231–237.
- [42] M.G. Pujar, N. Parvathavarthini, R.K. Dayal, S. Thirunavukkarasu, Assessment of intergranular corrosion (IGC) in 316(N) stainless steel using electrochemical noise (EN) technique, *Corros. Sci.* 51 (2009) 1707–1713.

- [43] T. Fukuda, T. Mizuno, The evaluation of pitting corrosion from the spectrum slope of noise fluctuation on iron and 304 stainless steel electrodes, *Corros. Sci.* 38 (1996) 1085–1091.
- [44] C.C. Lee, F. Mansfeld, Analysis of electrochemical noise data for a passive system in the frequency domain, *Corros. Sci.* 40 (1998) 959–962.
- [45] J. Feder, *Fractals*, Plenum Press, New York, 1988.
- [46] B.B. Mandelbrot, J.W. van Ness, Fractional Brownian motions, fractional noises and applications, *SIAM Rev.* 10 (1968) 422–437.
- [47] P.R. Roberge, D.R. Lenard, Characterization of corroding aluminium alloys with electrochemical noise and electrochemical impedance spectroscopy, *J. Appl. Electrochem.* 28 (1998) 405–410.
- [48] A. Horvath, R. Schiller, Rescaled range analysis of the corrosion potential noise, *Corros. Sci.* 45 (2003) 597–609.
- [49] A. Aballe, M. Bethencourt, F.J. Botana, M. Marcos, Using wavelets transform in the analysis of electrochemical noise data, *Electrochim. Acta* 44 (1999) 4805–4816.
- [50] J.A. Wharton, R.J.K. Wood, B.G. Mellor, Wavelet analysis of electrochemical noise measurements during corrosion of austenitic and superduplex stainless steels in chloride media, *Corros. Sci.* 45 (2003) 97–122.
- [51] C. Cai, Z. Zhang, F. Cao, Z. Gao, J. Zhang, C. Cao, Analysis of pitting corrosion behavior of pure Al in sodium chloride solution with the wavelet technique, *J. Electroanal. Chem.* 578 (2005) 143–150.
- [52] X.F. Liu, H.G. Wang, H.C. Gu, Fractal characteristic analysis of electrochemical noise with wavelet transform, *Corros. Sci.* 48 (2006) 1337–1367.
- [53] B.D. Malamud, D.L. Turcotte, Self-affine time series: measure of weak and strong persistence, *J. Stat. Plan. Infer.* 80 (1999) 173–196.
- [54] P. Planinšič, A. Petek, Characterization of corrosion processes by current noise wavelet-based fractal and correlation analysis, *Electrochim. Acta* 53 (2008) 5206–5214.
- [55] P. Flandrin, Wavelet analysis and synthesis of fractional Brownian motion, *IEEE Trans. Inf. Theory* 38 (1992) 910–916.
- [56] R. Holley, E. Waymire, Multifractal dimensions and scaling exponents for strongly bounded random cascades, *Ann. Appl. Probab.* 2 (1992) 819–845.
- [57] J.L. Véhel, R. Vojak, Multifractal analysis of Choquet capacities, *Adv. Appl. Math.* 20 (1998) 1–43.
- [58] C. Canus, J.L. Véhel, C. Tricot, Continuous large deviation multifractal spectrum: definition and estimation, in: M.M. Novak (Ed.), *Fractals and Beyond*, World Scientific, Singapore, 1998, pp. 117–128.
- [59] R.H. Riedi, Multifractal processes, in: P. Doukhan, G. Oppenheim, M.S. Taqqu (Eds.), *Theory and Applications of Long-Range Dependence*, Birkhuser, Basel, 2002, pp. 625–715.
- [60] I. Daubechies, *Ten Lectures on Wavelets*, SIAM, New York, 1992.
- [61] N.L. Johnson, S. Kotz, N. Balakrishnan, *Continuous Univariate Distributions*, vol. 1–2, John Wiley & Sons, New York, 1994.
- [62] T. Shibata, T. Takeyama, Pitting corrosion as a stochastic process, *Nature* 260 (1976) 315–316.
- [63] G.S. Frankel, Pitting corrosion of metals, *J. Electrochem. Soc.* 145 (1998) 2186–2198.
- [64] Y.F. Cheng, M. Wilmott, J.L. Luo, Analysis of the role of electrode capacitance on the initiation of pits for A516 carbon steel by electrochemical noise measurements, *Corros. Sci.* 41 (1999) 1245–1256.
- [65] R.A. Cottis, The interpretation of electrochemical noise data, *Corrosion* 27 (2001) 265–285.